Geomorphology 368 (2020) 107357

Contents lists available at ScienceDirect

Geomorphology

journal homepage: www.elsevier.com/locate/geomorph

Soil erosion changes during the last 30 years and contributions of gully erosion to sediment yield in a small catchment, southern China

Jing Liu [a,b], Honghu Liu [a,c,d,*]

[a] State Key Laboratory of Soil Erosion and Dryland Farming on the Loess Plateau, Institute of Soil and Water Conservation CAS and MWR, Yangling, Shannxi 712100, People's Republic of China
[b] University of Chinese Academy of Sciences, Beijing 100049, People's Republic of China
[c] Changjiang River Scientific Research Institute, Changjiang Water Resource Commission, Wuhan, Hubei Province 430010, People's Republic of China
[d] Research Center on Mountain Torrent & Geologic Disaster Prevention of the Ministry of Water Resources, Wuhan 430010, People's Republic of China

ARTICLE INFO

Article history:
Received 1 March 2020
Received in revised form 19 July 2020
Accepted 19 July 2020
Available online 23 July 2020

Keywords:
Sheet and rill erosion
Chinese Soil Loss Equation
Gully model
Sediment contribution

ABSTRACT

As a large weathered granite soil region in the world, southern China is experiencing severe sheet and rill erosion and gully erosion due to its special geological conditions, inappropriate land use, and high intensity precipitation. However, few studies have been conducted on the long-term dynamics of these two types of soil erosion and the sediment contribution of gully erosion in southern China. To assess this, estimates of soil erosion changes and the contribution ratio of gully erosion to sediment yield in a small catchment in southern China from 1989 to 2015 are quantified. A topographic map and three high-resolution satellite images were interpreted for land use changes to calculate soil erosion modulus of sheet and rill erosion by the Chinese soil loss equation (CSLE) and to estimate the amount of gully erosion by gully volume based on a generalized inverted triangular pyramid model multiplying bulk density. Results indicated that soil erosion modulus started as high as 10,442 t km^{-2} in 1989, followed by an initial decrease of 54% before increasing slightly. The total gully volume decreased by 37% overall, as did the cumulative amount of gully erosion. Between 2005 and 2010 positive total soil loss was calculated and the sediment contribution ratio of gully erosion was estimated to be 52.27%. It can be concluded that the combination of remote sensing images, the CSLE, and a new generalized gully model can effectively be used to quantify soil loss from sheet and rill erosion as well as gully erosion. This study provides a new insight to estimate gully erosion and the dynamic evolution of soil loss. Further studies should be performed in combination with field methods to validate this approach.

1. Introduction

Soil erosion is one of the most typical forms of land degradation worldwide, especially in areas with unfavorable environmental conditions such as special geology and heavy rainfall and areas with inappropriate land management practices (Borrelli et al., 2017; Deng et al., 2020; Zhang et al., 2020). These conditions are prominent in the weathered granite soil region of southern China where sheet and rill erosion and gully erosion exist simultaneously as two important types of soil erosion (Liang et al., 2009; Liao et al., 2018), and the sediment yield is high (Lin et al., 2015).

Soil erosion models have been effectively used to assess soil loss caused by sheet and rill erosion for individual land-use types and to develop soil and water conservation measures (Liu et al., 2002). Many empirical equations have been proposed and play an important role in predicting soil loss, which have the advantages of easy access to data, simple application, and GIS compatibility (Shi et al., 2004; Wu et al., 2019). Currently, the Universal Soil Loss Equation (USLE) (Wischmeier and Smith, 1978) and its improved version, the Revised Universal Soil Loss Equation (RUSLE) (Renard et al., 1997) are the most widely used empirical models. Taking into account three categories of systematic practices for soil and water conservation, Liu et al. (2002) introduced biological-control, engineering-control, and tillage practices (*B*, *E* and *T*, respectively) created during the development of Chinese agriculture traditions to replace the cover and management (*C*) and support practice (*P*) factors in the USLE and developed the Chinese Soil Loss Equation (CSLE). The CSLE has been used to quantitatively evaluate soil loss due to sheet and rill erosion in southern China (Chen et al., 2017; Duan et al., 2020; Li et al., 2020), but few studies have reported on its relationship with gully erosion.

Gully erosion is characterized by large amounts of sudden and intense erosion (Valentin et al., 2005; Liang et al., 2009). Studies have shown that gully erosion is the main threat to the security of ecology, food, flood control and human settlements in hilly areas, and has seriously restricted the sustainable development of local environments

* Corresponding author at: Changjiang River Scientific Research Institute, Changjiang Water Resource Commission, Wuhan, Hubei Province 430010, People's Republic of China.
E-mail address: liuhh@mail.crsri.cn (H. Liu).

https://doi.org/10.1016/j.geomorph.2020.107357
0169-555X/

and economies (Poesen et al., 2003; Liu et al., 2012). Ranked as one of the four most serious types of erosion ditches in China (Liu, 2018), gully erosion has become the most widespread, most vigorous, and most severe type of erosion in southern China based on field investigations and literature reports (Niu et al., 2000). Therefore, the study of gully erosion and its contribution to the sediment yield are of great significance to regional land management.

Gully volume reflects the amount of material removed from gully erosion (Woodward, 1999), which can be calculated by the differential thought method of multiplying the sum of gully cross-sections with lengths (Casalí et al., 2006). It is an ingenious choice to generalize the shape of the gully, which has the advantage of quick measurement (Casalí et al., 2006). Common generalizations are V-shaped, trapezoidal-shaped, and rectangular-shaped (Di Stefano et al., 2013; Luffman et al., 2015), with V-shaped gullies being dominant in the early stage of development, while trapezoidal-shaped cross-sections are predominant in permanent gullies (Ben Slimane et al., 2018). Based on the statistics of the field investigation data for catchments in southern China, the shape of the gullies should be generalized as an inverted triangular pyramid (Liu et al., 2015), and the inverted teardrop shape was a valid description of the gullies (Liu, 2018). However, little literature is available on measuring the gully erosion by the volume of generalized gully in southern China.

Research has shown that under many circumstances gully erosion is the main source of sediment at the catchment scale (Valentin et al., 2005; Vanmaercke et al., 2011). In Europe, contribution ratios of gully erosion to sediment yield were reported as 60.2% and 68.1% by Quine et al. (1994) and Martínez-Casasnovas et al. (2003), respectively, over several decades with a sharp increase to 90% during an exceptional rainfall event (Gaspar et al., 2019). In North Africa it was found that gully erosion contribution to total sediment ranges from 20% to 80% (Ben Slimane et al., 2016) but other studies have suggested that contributions of gully erosion account for less than 30% (Haregeweyn et al., 2017; Inoubli et al., 2017; Ben Slimane et al., 2018).

The sediment contribution of gully erosion has also been researched in China, with the loess region of north-western China contribution ratios of sediment production by gully erosion of 70% and 92.8%, respectively (Yang et al., 2006; Zhao et al., 2015), while an intermediate value of around 80% was reported in the hot, dry valley region of the Jinsha River (Zhang et al., 2017). These results indicate that the contribution of gully erosion to the total sediment yield cannot be ignored. Although research has been done on the contribution of gully erosion to the total soil erosion in many regions, little information is available in the weathered granite soil region of southern China, especially over long periods of time.

The specific objectives of this study are 1) to analyse the temporal and spatial changes in the annual average soil loss during the last 30 years using the CSLE, 2) to build a generalized model to calculate the gully volume (GV) using linear and areal gully parameters and to further assess the amount of gully erosion (AGE), and 3) to quantitatively estimate the sediment contribution of gully erosion to the total soil erosion in a small catchment of southern China. This study yields a long-term understanding of soil loss dynamics using remote sensing images, while the CSLE and generalized gully model provide feasible methods for quantifying soil erosion in the granitic region of southern China.

2. Material and methods

2.1. Study area

The study area is the Zuoma catchment, with an area of 0.73 km^2 located in Yudu County, Ganzhou district, Jiangxi Province, southern China (25.908°–25.920° N, 115.396°–115.406° E) (Fig. 1a). The Zuoma catchment belongs to the upper reaches of a tributary of the Ganjiang River, which is characterized by hilly topography and slope gradients ranging from 0° to 25°. It has a typical warm and humid subtropical monsoon climate with a mean annual precipitation of 1508 mm and an average annual temperature of 19.7 °C. The temporal distribution of precipitation in this region is uneven, with the majority of rainfall concentrated from April to June, which results in important soil erosion. The main soil type in the area is Orthic Acrisol, with a soil depth of about 1.0 m according to the Soil Survey Staff (Gong et al., 2002). The parent material is a weathering regolith of granite up to 20–60 m deep. The pH of the soil is between five and six. There is a river that originates from a pond in a paddy field and drains the catchment until its outlet. For more figures with field views of gullies and rill erosion, please see Liu et al. (2019).

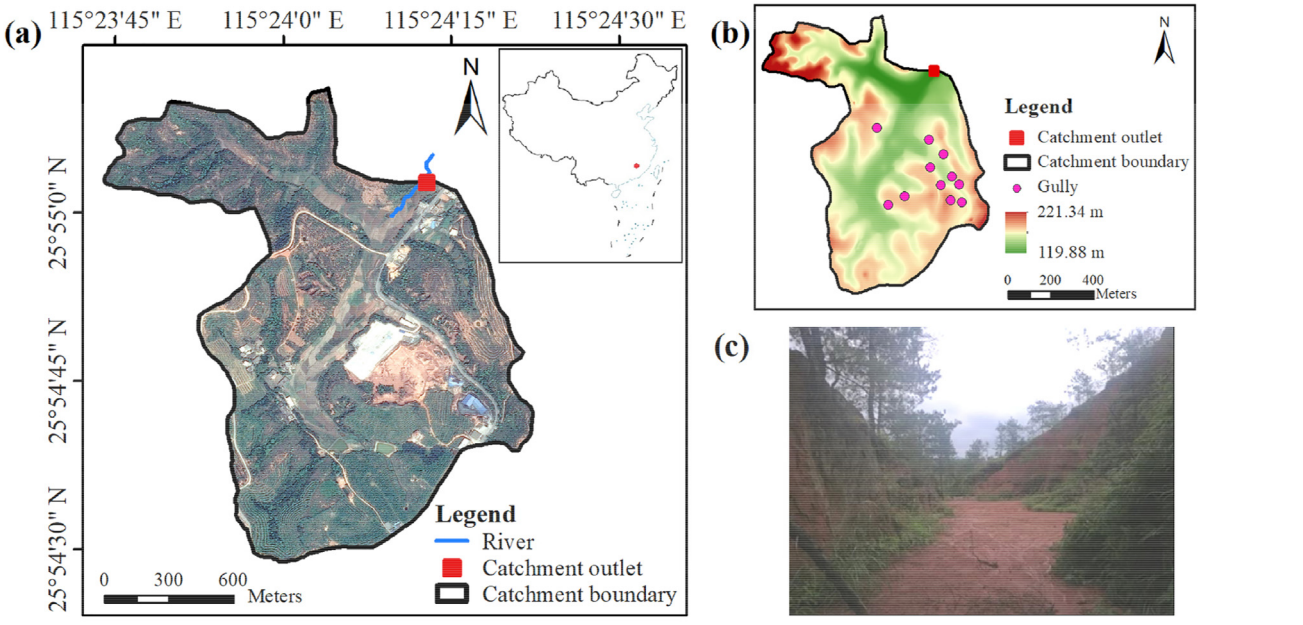

Fig. 1. (a) Location and landscape of the Zuoma catchment (Quickbird image from Apr. 2015), (b) digital elevation model showing distribution of gullies and (c) sedimentation evidence at the bottom of the gully (taken in Oct. 2018).

Since 1989, the Zuoma catchment has been classified as one of the Liupi Project Areas of the Key Soil and Water Loss Control Project in China (Wang et al., 2012). Thus, a series of soil and water conservation measures have been performed to improve the ecological conditions in the catchment.

2.2. Data processing

The work procedures consisted of data collection in the field and data analysis in the laboratory (Fig. 2). Four maps were collected for the research: a topographic map at 1:10,000 scale and a contour interval of 5 m made in July 1989 and three high-resolution QuickBird satellite images taken in April 2005, June 2010, and April 2015. Daily precipitation data were provided by the Yudu meteorological station. The DEM was derived from the Zuoma topographic map used in this study (Fig. 1b). The grid size of the DEM was set as 1 m. By combining the interpretation of the remote sensing images and the field survey, the distribution of the gullies during the last 30 years was delineated (Fig. 1b) and the gully boundary lines were extracted with the aim of displaying the development of gully parameters. Land-use status was obtained by interpreting the remote sensing images of the catchment and the area percentage of each land-use type during the study period was equal to the ratio of the area of a single type to the area of the catchment.

2.2.1. Calculation of soil loss due to sheet and rill erosion

To predict soil erosion this study uses a mathematical model-based method, the CSLE model. In the CSLE, the soil loss is expressed as follows (Liu et al., 2002):

$$A = R \times K \times LS \times B \times E \times T \quad (1)$$

where A is the average annual soil loss (t ha^{-1}); R is the rainfall erosivity factor (MJ mm h^{-1} ha^{-1}); K is the soil erodibility factor (t ha h ha^{-1} MJ^{-1} mm^{-1}); LS is the slope length and slope steepness factor, which is collectively known as the topographic factor (dimensionless); B is the biological-control factor; E is the engineering-control factor; and T is the tillage practices factor. B, E, and T, which are dimensionless, have a value range of 0–1 (Zhang and Liu, 2003). The smaller their values, the better the soil conservation benefit of a particular measure. The calculation methods of each factor are as follows.

(1) Rainfall erosivity factor (R)

Rainfall erosivity reflects the potential capacity of soil erosion caused by rainfall (Zhang et al., 2002). In this study, daily rainfall data from 1989 to 2015 were used to calculate the R factor (Fig. 3a) using Eq. (2), which was developed by Zhang et al. (2002):

$$M = \alpha \sum_{j=1}^{k} (P_j)^{\beta} \quad (2)$$

where M is the rainfall erosivity value of a half-month period (MJ mm h^{-1} ha^{-1}); k is the number of days in a half-month period; P_j is the erosive daily rainfall amount on the j-th day of the half-month period (mm), and α and β, calculated using Eqs. (3) and (4), respectively, are the undetermined parameters of the model:

$$\alpha = 21.586\beta^{-7.1891} \quad (3)$$

$$\beta = 0.8363 + \frac{18.177}{P_{d12}} + \frac{24.455}{P_{y12}} \quad (4)$$

where P_{d12} represents the average daily rainfall (mm) for a daily rainfall above 12 mm and P_{y12} represents the average annual rainfall (mm) for an annual rainfall above 12 mm.

(2) Soil erodibility factor (K)

Soil erodibility is an index used to evaluate the sensitivity of soil to erosion (Zhang et al., 2007). Based on the China Soil Database (http://vdb3.soil.csdb.cn/) and the parent material combined with land use, the soil types in the catchment were determined, which includes black-red sandy mud, thick red sandy mud, and

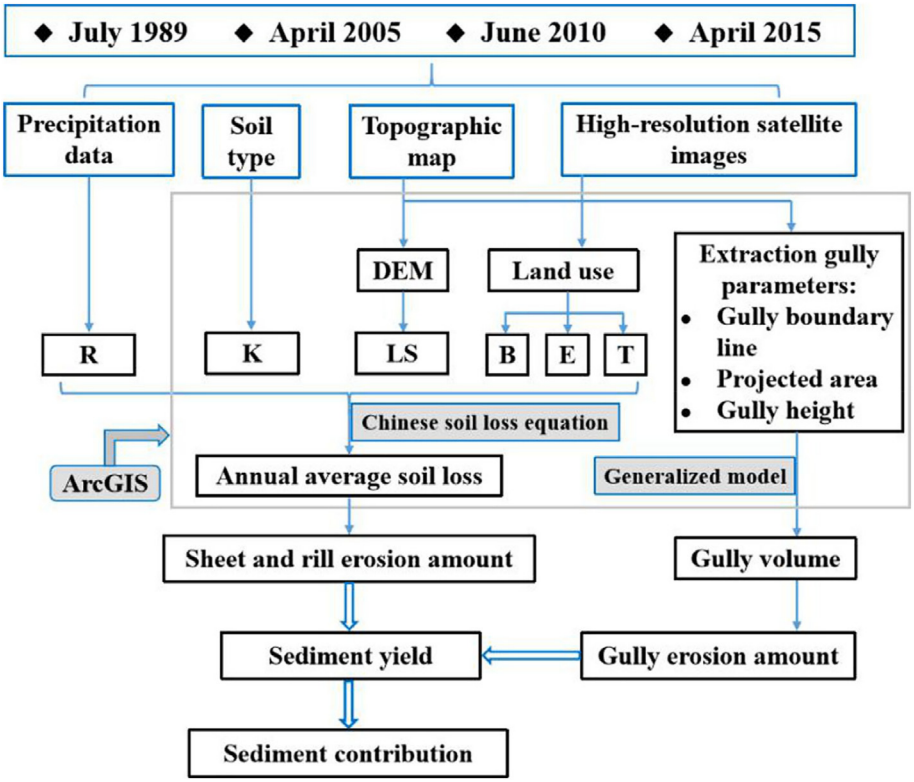

Fig. 2. Flow chart of data collection and processing.

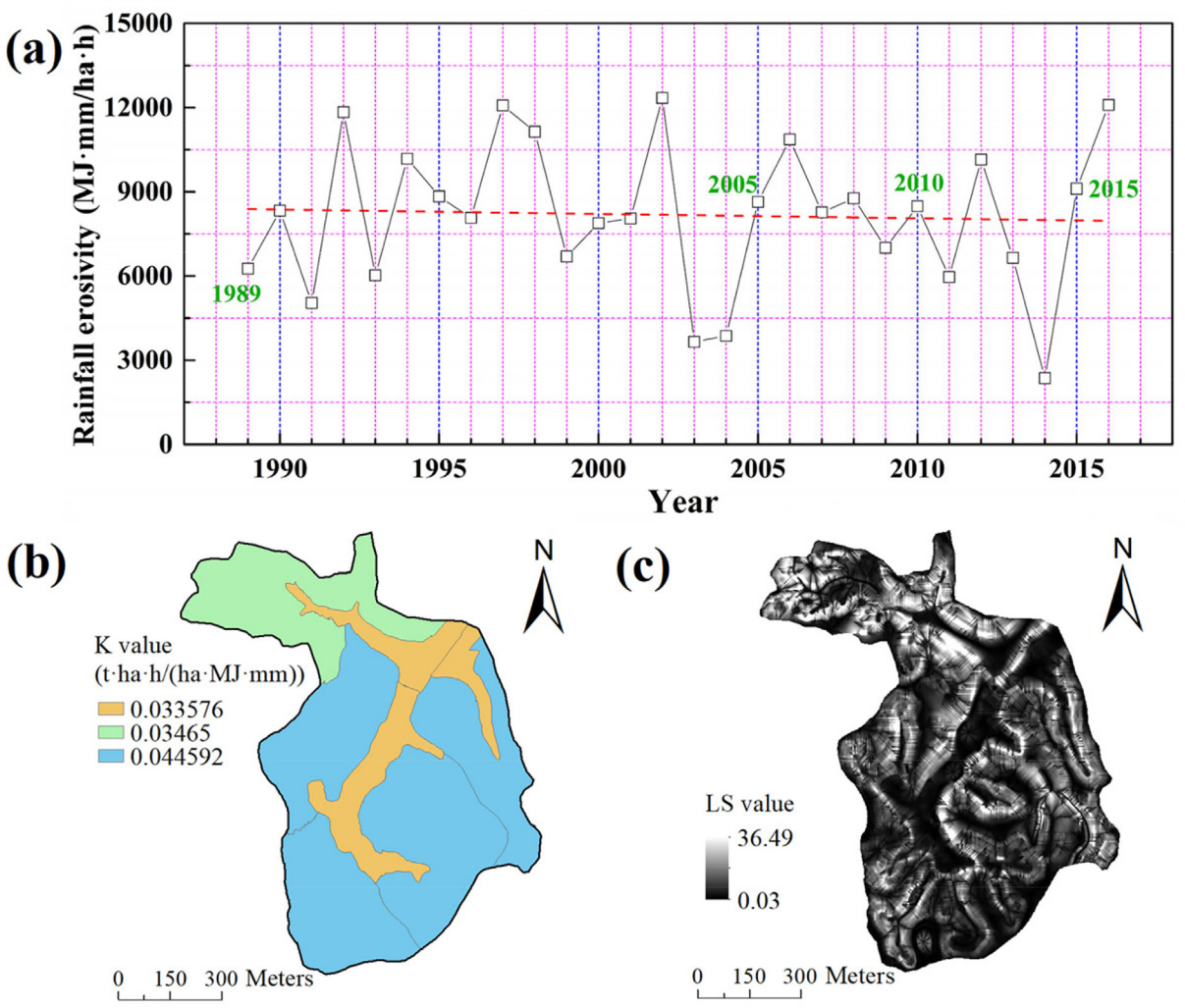

Fig. 3. (a) Annual rainfall erosivity from 1989 to 2015, (b) soil erodibility factor (*K*), and (c) topographic factor (*LS*) calculations for the Zuoma catchment.

red sandy mud. The *K* values of these three soil types are 0.033576, 0.044592 and 0.03465, respectively (Fig. 3b).

(3) Topographic factor (*LS*)

The topographic factor (*LS*), including the slope length (*L*) and the slope steepness (*S*), represents the ratio of soil loss under given conditions to that under standard conditions (slope of 9%, slope length of 22.13 m) (Wischmeier and Smith, 1978). The *LS* values (Fig. 3c) were calculated using the AML program provided by Hickey (2000) within the ArcGIS workstation, which includes the most suitable calculation method for gently rolling landscapes (Liu et al., 2011a). A horizontal resolution of 1 m was used in this study as it was the best fit for the accuracy of the *S* factor in Hickey's algorithm (Liu et al., 2009).

(4) Biological-control factor (*B*)

The biological-control factor (*B*) reflects the effect of biological cover on soil erosion. The assignment of forest in reference to the vegetation cover factor (*C*) value in the USLE follows the method used by Wischmeier and Smith (1978) and Wang and Jiao (1996). The soil conservation benefits of cultivated land are reflected by the *T* factor and the *B* assignment of the remaining land-use types refers to Wang et al. (2018) (Table 1). Fig. 4a illustrates the obtained *B* maps for the Zuoma catchment.

(5) Engineering-control factor (*E*)

The engineering-control factor (*E*) reflects the effects of engineering-control practices on soil loss. Engineering-control practices refer to the construction of terraces, silt dams, and other projects to change the topography in order to reduce runoff and soil erosion (Liu et al., 2002). In the study area, the terraces included earth dike terraces and stone dike terraces, with the *E* values of 0.414 and 0.084, respectively (Ministry of Water Resources of the People's Republic of China, 2018). And those of areas without soil and water conservation engineering measures were assigned a value of 1 (Fig. 4b).

Table 1
Biological-control factor (*B*) values of land-use types and forest coverage in the Zuoma catchment.

Land-use type		*B* value
Cultivated land		1
Rural residential area		0.025
Streets		0.01
Water bodies		0
Uncovered independent industrial & mining land		1
Forest	0% coverage	0.10
	20% coverage	0.08
	40% coverage	0.06
	60% coverage	0.02
	80% coverage	0.004
	100% coverage	0.001

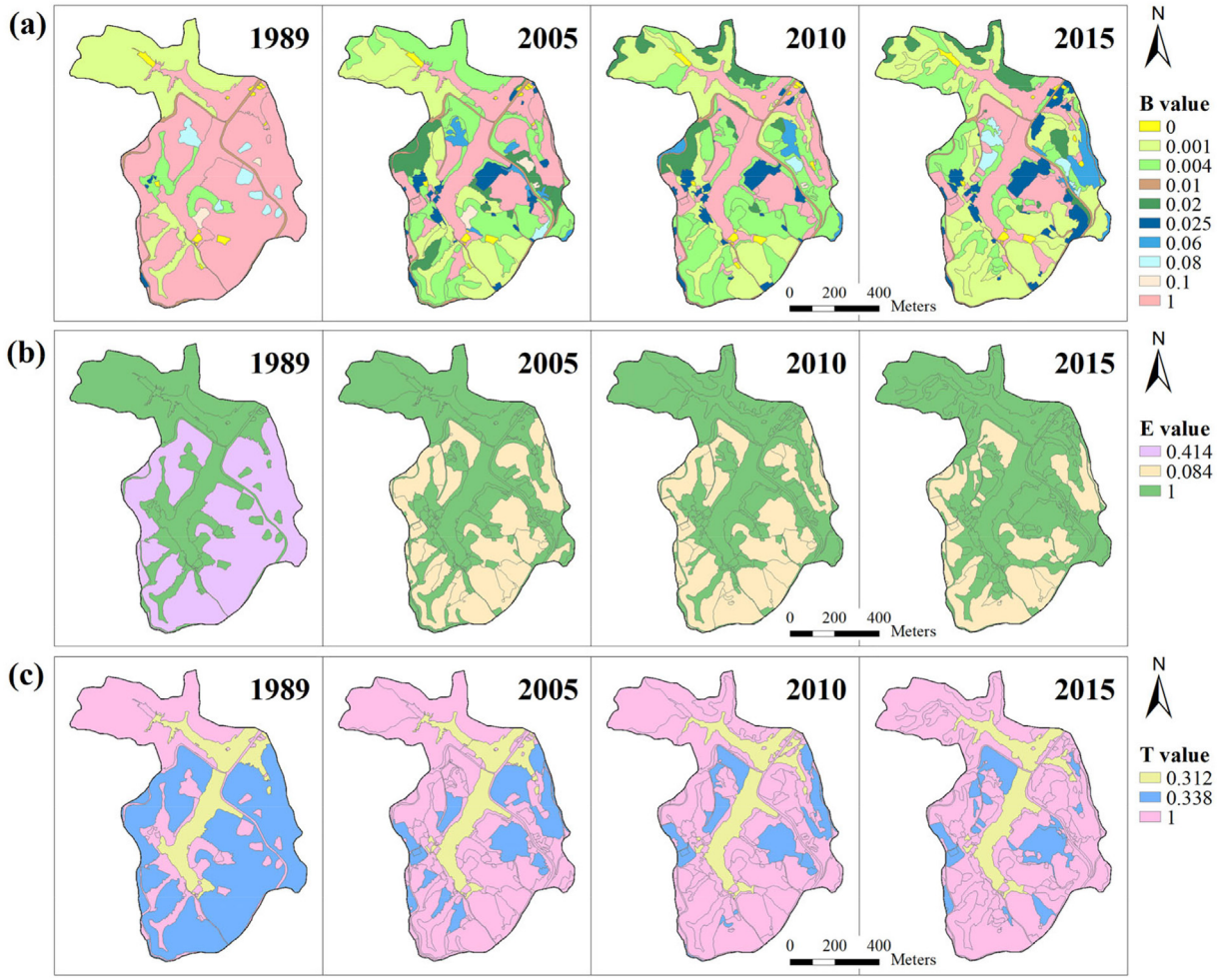

Fig. 4. (a) Biological-control factor (B), (b) engineering-control factor (E), and (c) tillage factor (T) calculations for the Zuoma catchment between 1989 and 2015.

(6) Tillage factor (T)
Tillage practices are measures of water retention and soil erosion prevention due to changing the micro-topography and increasing surface coverage through farming. The tillage factor (T) represents the ratio of the soil loss of certain tillage measures to the soil loss under the same conditions without tillage practices (Guo et al., 2013). In the study area, the T-factor assignments of the paddy field, which was part of the Two Lake Plain Hilly Paddy Field, Mid Triple-cropping, and Double-cropping Areas, and the dry land, which was part of the Nanling Hilly Mountains' Paddy Field, the Dry Land Double-cropping, and the Triple-cropping Areas, were 0.312 and 0.338, respectively (Ministry of Water Resources of the People's Republic of China, 2018). Other areas were assigned a value of 1 (Fig. 4c).

(7) Calculation of soil loss due to sheet and rill erosion
The vector layers of the K, B, E, and T factors mentioned above were converted into raster layers with a resolution of 1 m. By multiplying the R value and the raster layers of the LS factors, the soil erosion modulus at each grid point was determined for the period from 1989 and 2015. Then, the amount of sheet and rill erosion (ASR) in the catchment was calculated by multiplying the soil erosion modulus of each grid point with the grid size and accumulating the values. Average annual ASR (AASR) was equal to the ASR divided by a year, and the total soil erosion modulus for the entire study area was equal to the ASR divided by the area of catchment.

(8) Classification of the soil erosion intensity
According to the Standards for Classification and Gradation of Soil Erosion (SL190-2007) (Ministry of Water Resources of the People's Republic of China, 2008), the soil erosion modulus was classified into soil erosion intensities (Table 3), and the area and proportion of different soil erosion intensities were calculated. The calculations and analyses were implemented using ArcGIS 9.3, Origin 9.0, and Excel.

2.2.2. Calculating soil loss due to gully erosion

(1) Gully volume: An inverted triangular pyramid generalized model was established for calculating the volume of a gully (Fig. 5). The gully formed an erosional depression relative to the slope's surface. The plane of the original uneroded slope is the plane of the bottom of the triangular pyramid, and the slopes formed by erosion (i.e. the gully walls) are the sides of the pyramid. The vertical projection length L_m, which is the shortest horizontal distance from the gully head to the gully bottom, was measured using a distance measuring tool, and the area a_m was the result of the remote sensing interpretation. Accordingly, the length L of the gully along the original slope and the area a of the generalized triangular pyramid's bottom were calculated based on the relationship between the angle of the triangle and the side length of the area. The elevation data of the gully head and the gully bottom were extracted from the topographic map, with the difference being the gully's depth D_m. The slope of the bottom of the pyramid was obtained using the arctangent function and was represented by the letter α. The slope of the upper part of the ridge is larger (between 65° and 70°) with the slope of the lower edge of the wall being between 20° and 30° within the Zuoma catchment. The two slopes form the two

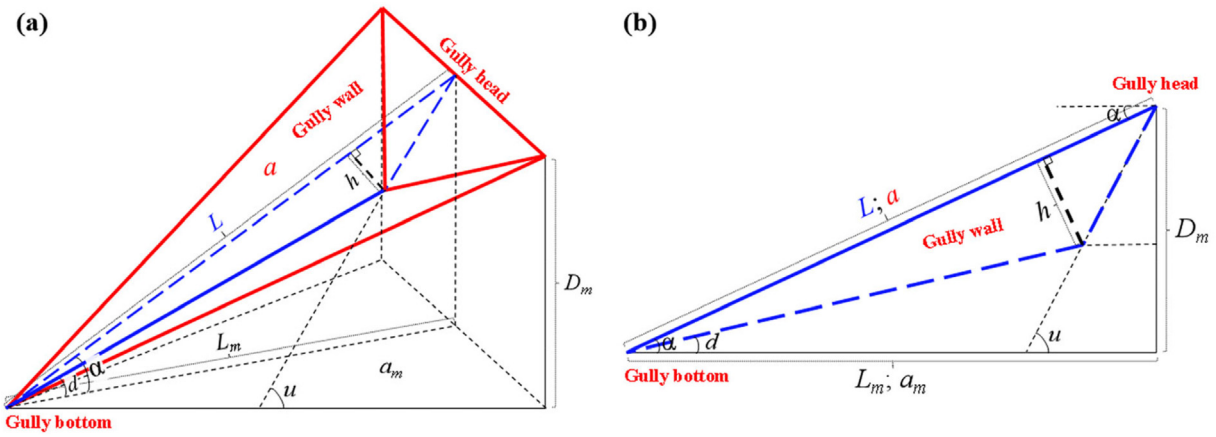

Fig. 5. Inverted triangular pyramid generalized gully model. (a) Illustrative diagram. (b) Front view.

sides of the triangular side view of the gully. In this study, the proper values of 67.5° and 20° were taken as the calculated values, respectively, and they were represented by the letters *u* and *d*, respectively. The convergence point of the two sides to the bottom edge was defined as the height *h*. The GV in each height interval was calculated based on the principle of similar triangles. The GV calculation formula of the generalized triangular pyramid is

$$V = \frac{1}{3} \times a \times h \tag{5}$$

where *V* is the volume of the generalized gully (m^3), *a* is the basal area of the generalized gully (m^2), and *h* is the height of the generalized triangular pyramid of the gully (m).

(2) Soil loss due to gully erosion: Three in situ soil samples were collected from each inner layer of the gully using a ring knife and the soil bulk density was determined using the gravimetric method. Except for the height of gully 8, which was the largest at 21.54 m in 1989 and the height of gully 3, which was between 16.30 m and 17.16 m from 2005 to 2015, the heights of all other gullies were less than 16 m. Therefore, the soil bulk density at depths of 0–16 m was determined from the field survey data and depths of greater than 16 m was assumed to be the same as that of the layer above (Table 2). The AGE was equal to the GV times the soil bulk density of the corresponding depth. The average annual AGE (AAGE) in 2005, 2010, and 2015 was calculated by dividing the inter annual difference by the number of years. The AAGE in 1989 was not be calculated because the initial development time of the gullies in 1989 cannot be determined.

2.3. Calculating the sediment contribution ratio of sheet and rill erosion and gully erosion

The sediment contribution ratio of sheet and rill erosion and gully erosion is the ratio of the AASR and AAGE to the total sediment yield, where the total sediment yield was estimated as the sum of AASR and AAGE.

3. Results

3.1. Land-use change during the last 30 years

The distribution map of land-use type is the premise for the *B*, *E*, and *T* factor assignments in the CSLE. Understanding the evolution of the land-use status over time (Fig. 6) is helpful in explaining the predicted soil loss. In 1989, sloping farmland was the main land-use type and mainly distributed on the southern slopes, accounting for 51.6% of the catchment area (Fig. 6b), while there were no orchards in the Zuoma catchment (Fig. 6a). Afterwards, the area of sloping farmland decreased dramatically due to land conversions into orchards, forests and building land, accounting for about 10% of the study area by 2015. Thus, forests and orchards were the dominant land-use types after 2005, accounting for more than 60% of the study area. The forests were concentrated in the mountainous areas in the northern part of the Zuoma catchment and scattered on some slopes in the southern part. The orchards, a majority of which are economic fruit forests, were mainly distributed on the southern slopes of hills, with the percentage of the area fluctuating slightly between 23.3% and 25.1%. The paddy fields, ranging from 0.0980 km^2 to 0.0890 km^2, were mainly distributed in the low terrain areas of the central catchment. The rural road, water, and unused land areas did not exhibit obvious inter-annual changes.

Table 2
Soil depth and soil bulk density (n = 3).

Soil depth (m)	0–0.3	0.3–3.0	3.0–7.0	7.0–12.0	12.0–16.0	>16.0
Bulk density (g cm^{-3})	1.44	1.67	1.71	1.73	1.79	1.79

3.2. Soil loss from sheet and rill erosion

The total soil erosion modulus was highest in 1989, which corresponds to extremely intense erosion (Table 3). After 16 years, the soil erosion modulus decreased sharply to a minimum value corresponding to moderate erosion. Then, as sheet and rill erosion intensified, the erosion moduli for 2010 and 2015 increased by 6.2% and 48.6%, respectively, compared with 2005, and it reached intense erosion levels. Specifically, the classification of the soil erosion modulus in the catchment is shown in Fig. 7. The area of micro-erosion was the largest, especially after 2005, reaching more than 50% of the catchment area (Fig. 7b), but the erosion amount of micro-erosion made the least contribution to the total ASR (Fig. 7c). The ASR corresponding to each soil erosion intensity increased significantly from micro-erosion to severe erosion. Severe erosion was the main contributor to the ASR of the Zuoma catchment for all study years, especially in 1989. Moreover, in terms of the proportion of the total area, severe erosion was only 2.5% smaller than micro-erosion and was widely distributed in the hillside outside the upstream mountainous area, while the latter was mainly located in the upstream mountainous area (Fig. 7a). In addition, the sediment contribution of each erosion intensity varied with time. Compared with 2010 and 2015, the contributions of the amount of the minimum and maximum erosion intensity in 2005 were lower (Fig. 7c). The amount with erosion modulus greater than 8000 t km^{-2} in 2015 was 51.8% higher than these in 2010 (Fig. 7c).

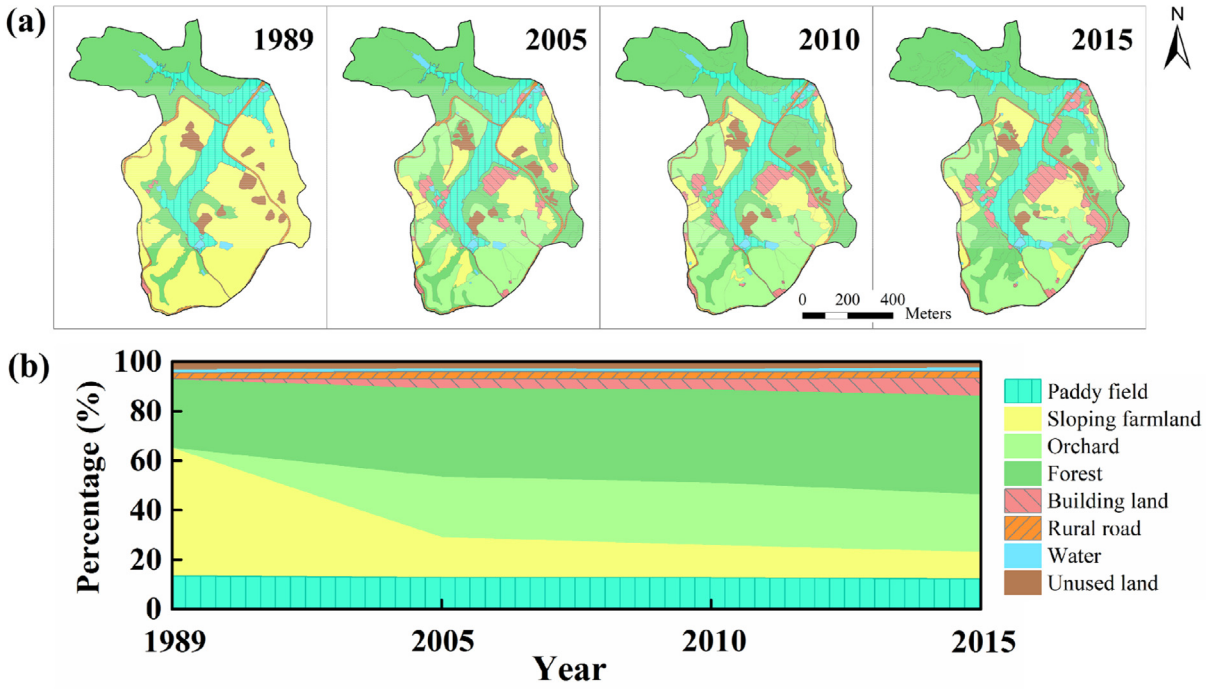

Fig. 6. Land-use changes in the Zuoma catchment from 1989 to 2015. (a) Distribution of land-use types. (b) Cumulative percentage of each land-use type.

3.3. Evolution of gully area and volume

The total area of all gullies developed in the catchment had a tendency to fluctuate and decrease over the last 30 years (Fig. 8a). Combined with Fig. 7a, 10 gullies developed in 1989, concentrated in the eastern portion, where the hilly area was wider and land cover was more sparse than that in the western side (Figs. 1b and 4a). Then, gullies 8, 9, 10, and 11 disappeared while gully 6 formed and gully 5 significantly developed, however the total gully area decreased by 20.1% in 2005. As time progressed, the area that the gullies covered increased from 2005 to 2010, but decreased to a minimum value in 2015. Additionally, the depths of most of the gullies decreased, especially the depth of gully 2, which reduced by 70% (Fig. 8b). Although gully 3 experienced minor fluctuations, it not only had the largest area, but also the maximum depth and the highest amount of gully erosion (Fig. 8c). For further details on the factors controlling the distribution of gullies across the Zuoma catchment the reader is directed to the work by Liu et al. (2019).

The total GV fell and rose, which was similar to the trend exhibited by the total gully area, but ultimately decreased by around 37% overall, as did the cumulative AGE. The total GV decreased by 30.9% from the maximum value in 1989 and 2005, after which, it exhibited a slight increase from 2005 to 2010 followed by another decrease from 2010 to 2015, ultimately decreasing by 37.0% of the maximum value in 1989 (Table 4). Gullies distributed in the same slope aspect had similar evolutionary trend although they are positioned on different hills. For example, gully 1 on the southern slope increased, along with gullies 4 and 5, while gully 2 on the northern slope was in the process of disappearing, along with gullies 10 and 11. Moreover, from 1989 to 2005 and from 2010 to 2015, the increase in the amount of sedimentation was greater than that of erosion in the gullies, that is, $|-78{,}555|$ t > 17,893 t and $|-32{,}062|$ t > 0 t, respectively (Fig. 8c), which means that the gullies were dominated by sedimentation below the slope and the AAGEs were negative in these two stages (Table 4). From 2005 to 2010, the AAGE increased by 7842 t year^{-1}, of which five gullies (1–5) experienced erosion and two gullies (6 and 7) experienced deposition.

Table 3
Soil erosion intensity classification and total sheet and rill erosion modulus of the Zuoma Catchment.

Year	Soil erosion modulus (t km^{-2})					
	0–500 (micro)	500–2500 (mild)	2500–5000 (moderate)	5000–8000 (intense)	8000–15,000 (extremely intense)	>15,000 (severe)
1989					10,442	
2005			4801			
2010				5097		
2015				7136		

3.4. Sediment contribution from gully erosion in the Zuoma catchment

Absolute values of the ratio of the AAGE change to the AASR change from 2005 to 2015 were far greater than 1 (Table 4), which indicates that the gully erosion has high instability. In addition, there was sedimentation in the gullies from 1989 to 2005 and from 2010 to 2015, while a positive AGE was calculated between 2005 and 2010 (Table 4). Thus, the sediment contribution ratio of gully erosion to total erosion was amounted to 52.3% from 2005 to 2010, indicating that the gully erosion was more severe than sheet and rill erosion.

4. Discussion

4.1. Suitability of calculating soil loss from sheet and rill erosion using the CSLE

This research attempted to estimate sheet and rill erosion and address the connection between the development of different land-use types and soil loss, which is necessary for soil and water conservation, land-use management, and eco-environmental construction. In this study, we assumed that the average annual soil loss from sheet and rill erosion could be effectively calculated by the CSLE and could reflect the relationship with land-use change. Compared with 1989, conversions of sloping farmland concentrated in hilly areas into forest and various citrus orchards led to a sharp decrease in soil loss for the period

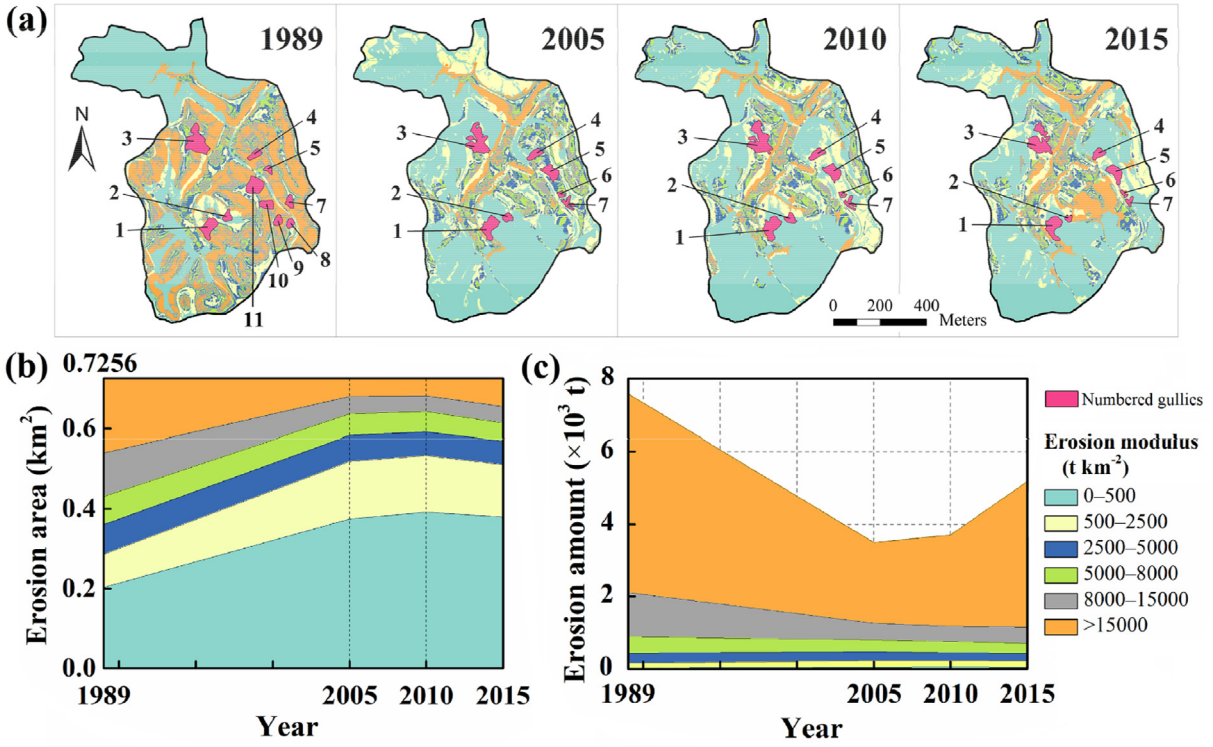

Fig. 7. (a) Distribution, (b) area and (c) amount of sheet and rill erosion for different erosion moduli in the Zuoma catchment. Gullies that developed in the catchment are also included in the maps.

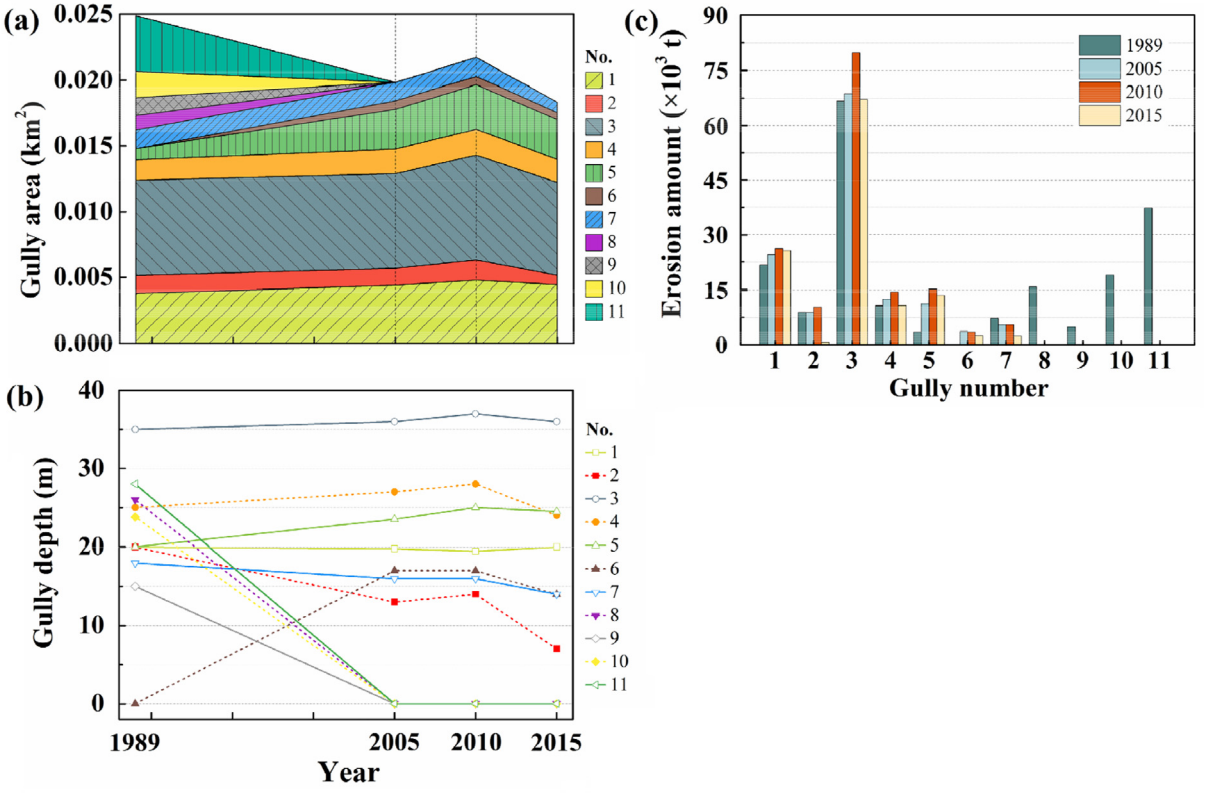

Fig. 8. Changes in the (a) gully area, (b) gully depth, and (c) amount of gully erosion of each gully from 1989 to 2015.

Table 4
Gully volume, amount of gully erosion (AGE), and relationships to the amount of sheet and rill erosion (ASR). The negative values represent that sedimentation is greater than erosion.

Year	Gully volume (m^3)	Cumulative AGE (t)	Average annual AGE (t $year^{-1}$)	Average annual AGE change/ASR change	Average annual ASR + AGE (t $year^{-1}$)	Sediment contribution from gully erosion (%)
1989	116,375	195,182	/	/	7576	/
2005	80,437	134,520	−3791	/	−308	/
2010	92,432	154,773	4051	36.58	7749	52.27
2015	73,374	122,711	−6412	−7.07	−1234	/

from 2005 and 2015. In the early stages, to improve the ecological environment, bring economic benefits, and further reduce sheet and rill erosion, sloping farmland was transitioned to orchards and forests, accounting for about one third of the study area. In general, forests and orchards have higher vegetation coverage than sloping farmland, and the corresponding *B* value is lower, which can effectively reduce soil and water loss (Sun et al., 2014). Moreover, the local residents in the Zuoma catchment changed the sloping farmland into terraces of earth dikes before 1989. Then, with the support of the government, earth dike terraces were further renovated as stone dike terraces between 1989 and 2005 to support large-scale orchards. Specific engineering control methods were given specific factor values to distinguish different types of soil erosion management, which was more suitable for national circumstances and used in the first China census of water (2010–2012). Since stone is more resistant than earth, stone dike terraces have a lower *E* value than earth dike terraces, and stone dike terraces are more effective than earth dike terraces in reducing the total surface runoff. In addition, tillage practices, namely cropping systems, incorporate specific times for harvest that are dependent on climate characteristics (Zhu et al., 2003). Tillage practices are regionally distinct, leading to realistic representation of local soil erosion. In this study, the changes to the *T* value were encapsulated in changes of other factors, so the impact of tillage practices on soil loss were not fully explored.

Mo et al. (2017) monitored gauging station data before and after the implementation of the national key construction project of soil and water conservation in the Zuoma catchment and found that the soil erosion intensity was moderate in 2003, which is close to the results of this study. After 2005, the soil loss increased, especially from 2010 to 2015. Although it was not as high as that in 1989, this obvious trend is worthy of attention. Specially, there was a large area of severe erosion (>15,000 t km^{-2}) in the middle right area of the catchment in 2015 (Fig. 7a). According to the field survey, the mountains in this area had been excavated, and thus, the vegetation and the soil covering the land surface were disturbed, resulting in the decrease of *B* value and the subsequent aggravation of sheet and rill erosion. However, the interpretation of the remote sensing images and the assignment of *B* are affected by subjective judgments, which may lead to errors in calculations. If the relative error can be controlled, which is easy to achieve, the continuous monitoring of land management combined with the calculation of soil loss by using remote sensing images and the CSLE model can provide a comprehensive understanding of the development of sheet and rill erosion.

4.2. Accuracy of the generalized gully volume

The GV and AGE calculated by the generalized triangular pyramid model reflect the status of gully erosion. Most of the gullies in the Zuoma catchment developed on hillsides, where the elevation changed significantly and the soil collapsed downward due to water erosion. The shapes of the gullies in this catchment are considered to be triangular pyramids (Liu et al., 2015). Although there are various techniques with specific characters surveying the GV, they have their own properties that are not suitable for this study. For instance, manual field investigations of the gullies provide detailed data, but often require more financial resources, manpower, and time. Long-term dynamic monitoring could not be easily carried out and is also subject to significant subjective influence (Liu et al., 2015). A high accuracy laser scanner was used to measure the morphology of the gully, however this method was not appropriate for gullies with a thick vegetation cover (Deng et al., 2016; Liu et al., 2019). In addition, the fingerprinting approach has been widely applied in sediment monitoring at different spatiotemporal scales (Wasson et al., 2002; Ben Slimane et al., 2013; Lin et al., 2015). While it is limited by sample size, sampling environment, and transport behaviour, care must be taken to collect samples immediately following events (Koiter et al., 2013; McCarney-Castle et al., 2017).

The results of this study were obtained using the generalized shape method, which can draw support from field assessments, satellite images, and DEMs. Poesen et al. (1996) reported that the volume extracted from aerial photographs was in good agreement with the data obtained through field monitoring. The method is capable of obtaining the process over a historical period, of broadening the geographical scope, and of lengthening the spatiotemporal scale of the project since another study of gullies in this area has shown that the gullies are still active (Liu et al., 2019). Since some small gullies were not evaluated if the spatial resolution was low (e.g. 5 m), very high spatial resolution images (e.g., 0.61 m) used in this study are considered to be better for measuring erosion (Tebebu et al., 2010; Taguas et al., 2012; Li et al., 2015), with the advantages of convenient operation, less field survey burden, calculation of volume over mid- to long-term temporal scales, and improvement of the accuracy of gully identification (Desprats et al., 2013; Ben Slimane et al., 2018). Although the representative shape was selected subjectively by the observer and may lead to errors (Casalí et al., 2006; Liu et al., 2015), the generalized gully model may be a valuable tool for improving the understanding of the characteristics of gully evolution.

4.3. Contribution of gully erosion to the sediment yield

From 2005 to 2010, gully erosion was the predominant contributor to the total sediment delivery for the weathered granite soil region in southern China, while there was no dynamic evolution of the contribution ratio during the last 30 years. The Zuoma catchment is a typical representation of land management policies containing the common land use types in Jiangxi province (Zhang et al., 2011), with the gully area accounting for 2.5%–3.4% of the total study area, close to the research results of Liu et al. (2020) at the regional scale in southern China. Moreover, as described in Section 3.3, there were gullies in different developmental states (disappearing, forming, and developing). Although the study area is small, it is representative and can be used as a case study for all of southern China.

The erosion of a gully is accompanied by an increase in the area and/or depth of the gully, while sedimentation in a gully is accompanied by a decrease in the area and/or depth (Fig. 8). For active gullies, sedimentation below the slope and erosion on the slope occur simultaneously. The increase and decrease in the cumulative AGE means that the gully is dominated by erosion and sedimentation, respectively. From 1989 to 2005 and from 2010 to 2015, six gullies (2 and 7–11) and seven gullies (1–7) experienced sedimentation, respectively, while five gullies (1 and 3–6) and zero gullies, respectively, experienced erosion over the same time periods (Fig. 8c). Thus, the amount of sedimentation offset the amount of erosion indicating that there was no net erosion in these two periods. In addition, artificial construction promotes the deposition

of sediment at the bottom of gullies, as revealed in a field survey conducted on gully 3 with a check dam in October 2018. The bottom of the gully has experienced deposition for several years (Fig. 1c), confirming the quantitative results in this paper. What's more, the implementation of protective measures such as upper intercepting, middle cutting, lower blocking, and internal and external greening (Liang et al., 2009) has alleviated gully erosion after 2010, increasing the role of sedimentation. Our evaluation is in agreement with Taguas et al. (2012), who determined that about half of the sediment sources were gully contributions in Spain, and Zhang et al. (2017), who noted that gully erosion was the main process causing soil loss and land degradation in southwestern China. However, there is still a need for the verification and calibration of field monitoring data that should be carried out for more precise investigation of gullies, especially when remote sensing images are used to measure gullies (Liu et al., 2011b). Therefore, future studies of sediment contribution should combine remote sensing with field monitoring to further investigate erosion. In addition, it is necessary to further study the targeted prevention and control measures of the sheet and rill erosion, which accounted for nearly half of the sediment yield contribution in this evaluation.

5. Conclusions

This study provides information on the soil loss dynamics during the last 30 years and contributions of gully erosion to sediment yield in a catchment of the weathered granite soil region in southern China. The CSLE model was utilized to estimate the soil loss from sheet and rill erosion, and addressed relationships between land-use status interpreted from remote sensing images and soil erosion. It was found that sloping farmland led to severe soil erosion, and conversions of sloping farmland into forests and orchards with higher vegetation coverage as well as engineering-control measures decreased soil loss effectively, indicating that the CSLE was suitable for predicting sheet and rill erosion. A new triangular pyramid generalized model was proposed and successfully used to identify the evolution of gully erosion. Results indicated that GV and AGE decreased during the last 30 years, which was verified by the deposition on gully observed in the field, thus confirming the accuracy of the proposed gully model calculation. The contribution ratio of gully erosion to the total sediment yield was 52.27% from 2005 to 2010, which suggested that gully erosion was the predominant contributor to total soil erosion for the catchment in the granitic region of southern China. The present study highlights that the combination of remote sensing, CSLE, and triangular pyramid generalized gully model is effective for quantifying the spatiotemporal evolution of soil erosion and relationships between sediment from different sources. However, valuable new gully model calculations and the use of remote sensing should be further confirmed in future research with field validation.

Declaration of competing interest

The authors declare that they have no known competing financial interests or personal relationships that could have appeared to influence the work reported in this paper.

Acknowledgments

This research was supported by the National Key Research and Development Program of China (Grant No. 2017YFE0118100-2), National Natural Science Foundation of China (Grant No. 413101297) and the One Hundred Person Project of Shaanxi Province (Grant No. [2017] 35). We thank Prof. Dr. Baoyuan Liu and Dr. Georg Hörmann for providing reviews to this manuscript and Dr. Longxi Cao for helping us to determine the value of the soil erodibility factor.

References

Ben Slimane, A., Raclot, D., Evrard, O., Sanaa, M., Lefèvre, I., Ahmadi, M., Tounsi, M., Rumpel, C., Ben Mammou, A., Le Bissonnais, Y., 2013. Fingerprinting sediment sources in the outlet reservoir of a hilly cultivated catchment in Tunisia. J. Soils Sediments 13 (4), 801–815. https://doi.org/10.1007/s11368-012-0642-6.

Ben Slimane, A., Raclot, D., Evrard, O., Sanaa, M., Lefevre, I., Le Bissonnais, Y., 2016. Relative contribution of rill/interrill and gully/channel erosion to small reservoir siltation in mediterranean environments. Land Degrad. Dev. 27 (3), 785–797. https://doi.org/10.1002/ldr.2387.

Ben Slimane, A., Raclot, D., Rebai, H., Le Bissonnais, Y., Planchon, O., Bouksila, F., 2018. Combining field monitoring and aerial imagery to evaluate the role of gully erosion in a Mediterranean catchment (Tunisia). Catena 170, 73–83. https://doi.org/10.1016/j.catena.2018.05.044.

Borrelli, P., Robinson, D.A., Fleischer, L.R., Lugato, E., Ballabio, C., Alewell, C., Meusburger, K., Modugno, S., Schutt, B., Ferro, V., Bagarello, V., Oost, K.V., Montanarella, L., Panagos, P., 2017. An assessment of the global impact of 21st century land use change on soil erosion. Nat. Commun. 8 (2013). https://doi.org/10.1038/s41467-017-02142-7.

Casalí, J., Loizu, J., Campo, M.A., De Santisteban, L.M., Álvarez-Mozos, J., 2006. Accuracy of methods for field assessment of rill and ephemeral gully erosion. Catena 67 (2), 128–138. https://doi.org/10.1016/j.catena.2006.03.005.

Chen, M.Q., Wei, X., Zhang, K.L., Chen, Y.H., 2017. Analysis of the characteristics of soil and water loss in Guizhou province based on CSLE. Journal of Soil and Water Conservation 31 (3), 16–21. https://doi.org/10.13870/j.cnki.stbcxb.2017.03.003 (26, in Chinese with English abstract).

Deng, Q.C., Qin, F.C., Zhang, B., Wang, H.P., Luo, M.L., Shu, C.Q., Liu, Hui, Gang, Cai, Liu, 2016. Characterizing the morphology of gully cross-sections based on PCA: a case of Yuanmou Dry-Hot Valley. Geomorphology 228, 703–713. https://doi.org/10.1016/j.geomorph.2014.10.032.

Deng, L.Z., Sun, T.Y., Fei, K., Zhang, L.P., Fan, X.J., Wu, Y.H., Ni, L., 2020. Effects of erosion degree, rainfall intensity and slope gradient on runoff and sediment yield for the bare soils from the weathered granite slopes of SE China. Geomorphology 352. https://doi.org/10.1016/j.geomorph.2019.106997.

Desprats, J.F., Raclot, D., Rousseau, M., Cerdan, O., Garcin, M., Le Bissonnais, Y., Ben Slimane, A., Fouche, J., Monfort-Climent, D., 2013. Mapping linear erosion features using high and very high resolution satellite imagery. Land Degrad. Dev. 24 (1), 22–32. https://doi.org/10.1002/ldr.1094.

Di Stefano, C., Ferro, V., Pampalone, V., Sanzone, F., 2013. Field investigation of rill and ephemeral gully erosion in the Sparacia experimental area, South Italy. Catena 101, 226–234. https://doi.org/10.1016/j.catena.2012.10.012.

Duan, X.W., Bai, Z.W., Rong, L., Li, Y.B., Ding, J.H., Tao, Y.Q., Li, J.X., Li, J.S., Wang, W., 2020. Investigation method for regional soil erosion based on the Chinese Soil Loss Equation and high-resolution spatial data: case study on the mountainous Yunnan Province, China. Catena 184. https://doi.org/10.1016/j.catena.2019.104237.

Gaspar, L., Lizaga, I., Blake, W.H., Latorre, B., Quijano, L., Navas, A., 2019. Fingerprinting changes in source contribution for evaluating soil response during an exceptional rainfall in Spanish pre-pyrenees. J. Environ. Manag. 240, 136–148. https://doi.org/10.1016/j.jenvman.2019.03.109.

Gong, Z.T., Zhang, G.L., Chen, Z.C., Luo, G.B., Zhao, W.J., 2002. Soil reference on the bases of chinese soil taxonomy. Chinese Journal of Soil Science 33 (1), 1–5. https://doi.org/10.19336/j.cnki (in Chinese with English abstract).

Guo, Q.K., Liu, B.Y., Zhu, S.B., Wang, G.Y., Liu, Y.N., Wang, A.J., 2013. Main factors of soil and water conservation tillage measures in China. Soil and Water Conservation in China 10, 22–26. https://doi.org/10.14123/j.cnki.swcc.2013.10.009 (in Chinese).

Haregeweyn, N., Tsunekawa, A., Poesen, J., Tsubo, M., Meshesha, D.T., Fenta, A.A., Nyssen, J., Adgo, E., 2017. Comprehensive assessment of soil erosion risk for better land use planning in river basins: case study of the Upper Blue Nile River. Sci. Total Environ. 574, 95–108. https://doi.org/10.1016/j.scitotenv.2016.09.019.

Hickey, R., 2000. Slope angle and slope length solutions for GIS. Cartography 29 (1), 1–8. https://doi.org/10.1080/00690805.2000.9714334.

Inoubli, N., Raclot, D., Mekki, I., Moussa, R., Le Bissonnais, Y., 2017. A spatiotemporal multiscale analysis of runoff and erosion in a Mediterranean Marly Catchment. Vadose Zone J. 16 (12). https://doi.org/10.2136/vzj2017.06.0124.

Koiter, A.J., Owens, P.N., Petticrew, E.L., Lobb, D.A., 2013. The behavioural characteristics of sediment properties and their implications for sediment fingerprinting as an approach for identifying sediment sources in river basins. Earth Sci. Rev. 125, 24–42. https://doi.org/10.1016/j.earscirev.2013.05.009.

Li, Z., Zhang, Y., Zhu, Q.K., He, Y.M., Yao, W.J., 2015. Assessment of bank gully development and vegetation coverage on the Chinese Loess Plateau. Geomorphology 228, 462–469. https://doi.org/10.1016/j.geomorph.2014.10.005.

Li, Z.W., Ning, K., Chen, J., Liu, C., Wang, D.Y., Nie, X.D., Hu, X.Q., Wang, L.X., Wang, T.W., 2020. Soil and water conservation effects driven by the implementation of ecological restoration projects: evidence from the red soil hilly region of China in the last three decades. J. Clean. Prod., 260 https://doi.org/10.1016/j.jclepro.2020.121109.

Liang, Y., Ning, D.H., Pan, X.Z., Li, D.C., Zhang, B., 2009. Characteristics and management of gully erosion in red soil area of South China. Soil Water Conserv. China 1, 31–34. https://doi.org/10.3969/j.issn.1000-0941.2009.01.010 (in Chinese).

Liao, Y.S., Tang, C.Y., Yuan, Z.J., Zhuo, M.N., Huang, B., Nie, X.D., Xie, Z.Y., Li, D.Q., 2018. Research progress on Benggang erosion and its prevention measure in red soil region of southern China. Acta Pedologica Sinica 55 (6), 1297–1312. https://doi.org/10.11766/trxb201807030219 (in Chinese with English abstract).

Lin, J.S., Huang, Y.H., Wang, M.-K., Jiang, F.S., Zhang, X.B., Ge, H.L., 2015. Assessing the sources of sediment transported in gully systems using a fingerprinting approach: an example from south-east China. Catena 129, 9–17. https://doi.org/10.1016/j.catena.2015.02.012.

Liu, X.L., 2018. Benggang erosion landform and research progress in a global perspective. Progress in Geography 37 (3), 342–351. https://doi.org/10.18306/dlkxjz.2018.03.005 (in Chinese with English abstract).
Liu, B.Y., Zhang, K.L., Xie, Y., 2002. An empirical soil loss equation. 12th ISCO Conference, Beijing.
Liu, H.H., Fohrer, N., Hörmann, G., Kiesel, J., 2009. Suitability of S factor algorithms for soil loss estimation at gently sloped landscapes. Catena 77 (3), 248–255. https://doi.org/10.1016/j.catena.2009.02.001.
Liu, H.H., Kiesel, J., Hörmann, G., Fohrer, N., 2011a. Effects of DEM horizontal resolution and methods on calculating the slope length factor in gently rolling landscapes. Catena 87 (3), 368–375. https://doi.org/10.1016/j.catena.2011.07.003.
Liu, H.H., Liu, X.C., Zhang, P.C., Wang, Y.F., 2011b. Characteristics of slope collapse and its monitoring technology in Southern China. Science of Soil and Water Conservation 9 (2), 19–23. https://doi.org/10.16843/j.sswc.2011.02.004 (in Chinese with English abstract).
Liu, H.H., Zhang, T.Y., Liu, B.Y., Liu, G., Wilson, G.V., 2012. Effects of gully erosion and gully filling on soil depth and crop production in the black soil region, northeast China. Environ. Earth Sci. 68 (6), 1723–1732. https://doi.org/10.1007/s12665-012-1863-0.
Liu, H.H., Qin, F., Chen, J., Liu, Z.H., Ding, W.F., 2015. Accuracy of slope collapse data collected by artificial survey. J. Yangtze River Sci. Res. Inst. 32 (3), 117–120. https://doi.org/10.3969/j.issn.1001-5485.2015.03.023 (in Chinese with English abstract).
Liu, H.H., Qian, F., Ding, W.F., Gómez, J.A., 2019. Using 3D scanner to study gully evolution and its hydrological analysis in the deep weathering of southern China. Catena 183. https://doi.org/10.1016/j.catena.2019.104218.
Liu, H.H., Hörmann, G., Qi, B.Y., Yue, Q.X., 2020. Using high-resolution aerial images to study gully development at the regional scale in southern China. Int. Soil Water Conserv. Res. https://doi.org/10.1016/j.iswcr.2020.03.004.
Luffman, I.E., Nandi, A., Spiegel, T., 2015. Gully morphology, hillslope erosion, and precipitation characteristics in the Appalachian Valley and Ridge province, southeastern USA. Catena 133, 221–232. https://doi.org/10.1016/j.catena.2015.05.015.
Martínez-Casasnovas, J.A., Antón-Fernández, C., Ramos, M.C., 2003. Sediment production in large gullies of the Mediterranean area (NE Spain) from high resolutions DEMs and GIS analysis. Earth Surf. Process. Landf. 28, 443–456. https://doi.org/10.1002/esp.451.
McCarney-Castle, K., Childress, T.M., Heaton, C.R., 2017. Sediment source identification and load prediction in a mixed-use Piedmont watershed, South Carolina. J. Environ. Manag. 185, 60–69. https://doi.org/10.1016/j.jenvman.2016.10.036.
Ministry of Water Resources of the People's Republic of China, 2008. Standards for Classification and Gradation of Soil Erosion, SL190-2007 (Beijing, China, in Chinese).
Ministry of Water Resources of the People's Republic of China, 2018. Technical Regulation for Dynamic Detection of Regional Soil Erosion (Beijing, China, in Chinese).
Mo, M.H., Fang, S.W., Yang, J., Song, Y.J., 2017. Soil and water control model and its environmental benefit analysis in small watershed of red soil. Jiangsu Agricultural Sciences 45 (7), 284–286. https://doi.org/10.15889/j.issn.1002-1302.2017.07.074 (311, in Chinese).
Niu, D.K., Guo, X.M., Zuo, C.Q., Li, X.X., 2000. Analysis of the distribution and environmental surroundings of collapsed hills land of red soil in south of China. Acta Agriculturae Universitatis Jiangxiensis 22 (2), 204–208 (doi:10.13836/j.j, in Chinese with English abstract).
Poesen, J., Vandaele, K., Van Wesemael, B., 1996. Contribution of gully erosion to sediment production in cultivated lands and rangelands. IAHS Publ. 236, 251–266.
Poesen, J., Nachtergaele, J., Verstraeten, G., Valentin, C., 2003. Gully erosion and environmental change: importance and research needs. Catena 50, 91–133. https://doi.org/10.1016/S0341-8162(02)00143-1.
Quine, T.A., Desmet, P.J.J., Govers, G., Vandaele, K., Walling, D.E., 1994. A comparison of the roles of tillage and water erosion in landform development and sediment export on agricultural land near Leuven, Belgium. IAHS Publ. 224, 77–86.
Renard, K.G., Foster, G.R., Weesies, G.A., Mccool, D.K., Yoder, D.C., 1997. Predicting soil erosion by water: a guide to conservation planning with the Revised Universal Soil Loss Equation (RUSLE). Agric Handb Us Dep Agric.
Shi, Z.H., Cai, C.F., Ding, S.W., Wang, T.W., Chow, T.L., 2004. Soil conservation planning at the small watershed level using RUSLE with GIS: a case study in the Three Gorge Area of China. Catena 55 (1), 33–48. https://doi.org/10.1016/s0341-8162(03)00088-2.
Sun, W.Y., Shao, Q.Q., Liu, J.Y., Zhai, J., 2014. Assessing the effects of land use and topography on soil erosion on the Loess Plateau in China. Catena 121, 151–163. https://doi.org/10.1016/j.catena.2014.05.009.
Taguas, E.V., Yuan, Y., Bingner, R.L., Gómez, J.A., 2012. Modeling the contribution of ephemeral gully erosion under different soil managements: a case study in an olive orchard microcatchment using the AnnAGNPS model. Catena 98, 1–16. https://doi.org/10.1016/j.catena.2012.06.002.
Tebebu, T.Y., Abiy, A.Z., Zegeye, A.D., Dahlke, H.E., Easton, Z.M., Tilahun, S.A., Collick, A.S., Kidnau, S., Moges, S., Dadgari, F., Steenhuis, T.S., 2010. Surface and subsurface flow effect on permanent gully formation and upland erosion near Lake Tana in the northern highlands of Ethiopia. Hydrol. Earth Syst. Sci. 14 (11), 2207–2217. https://doi.org/10.5194/hess-14-2207-2010.
Valentin, C., Poesen, J., Li, Y., 2005. Gully erosion: impacts, factors and control. Catena 63 (2–3), 132–153. https://doi.org/10.1016/j.catena.2005.06.001.
Vanmaercke, M., Poesen, J., Verstraeten, G., Maetens, W., de Vente, J., 2011. Sediment yield as a desertification risk indicator. Sci. Total Environ. 409, 1715–1725. https://doi.org/10.1016/j.scitotenv.2011.01.034.
Wang, W.Z., Jiao, J.Y., 1996. Quantitive evaluation on factors influencing soil erosion in China. Bull. Soil Water Conserv. 16 (5), 1–20 (in Chinese with English abstract).
Wang, B.W., Xiao, S.S., Zhang, G.H., Yang, J., Zhang, L.C., 2012. Study on runoff and sediment yield characteristics under different land uses in red soil area of Southern China. Trans. CSAE 28 (2), 239–243. https://doi.org/10.3969/j.issn.1002-6819.2012.02.041 (in Chinese with English abstract).
Wang, L., Qu, C., Zhao, G.D., 2018. Quantitative assessment of regional soil erosion based on Chinese soil loss equation model. Bulletin of Soil and Water Conservation 38 (1), 122–130. https://doi.org/10.13961/j.cnki.stbctb.2018.01.021 (in Chinese with English abstract).
Wasson, R.J., Caitcheon, G., Murray, A.S., McCulloch, M., Quade, J., 2002. Sourcing sediment using multiple tracers in the catchment of Lake Argyle, northwestern Australia. Environ. Manag. 29 (5), 634–646. https://doi.org/10.1007/s00267-001-0049-4.
Wischmeier, W.H.A., Smith, D.D., 1978. Predicting rainfall erosion losses: a guide to conservation planning. Agricultural Handbook No. 537. U.S. Department of Agriculture, Washington, DC.
Woodward, D.E., 1999. Method to predict cropland ephemeral gully erosion. Catena 37, 393–399. https://doi.org/10.1016/s0341-8162(99)00028-4.
Wu, H., Li, Z., Clarke, K.C., Shi, W.Z., Fang, L.C., Lin, A.Q., Zhou, J., 2019. Examining the sensitivity of spatial scale in cellular automata Markov chain simulation of land use change. Int. J. Geogr. Inf. Sci. 33 (5), 1040–1061. https://doi.org/10.1080/13658816.2019.1568441.
Yang, M.Y., Tian, J.L., Liu, P.L., 2006. Investigating the spatial distribution of soil erosion and deposition in a small catchment on the Loess Plateau of China, using 137Cs. Soil Tillage Res. 87 (2), 186–193. https://doi.org/10.1016/j.still.2005.03.010.
Zhang, W.B., Liu, B.Y., 2003. Development of Chinese Soil Loss Equation Information System based on GIS. Journal of Soil and Water Conservation 17 (2), 89–92 (doi:CNKI:SUN:TRQS.0.2003-02-025, in Chinese with English abstract).
Zhang, W.B., Xie, Y., Liu, B.Y., 2002. Rainfall erosivity estimation using daily rainfall amounts. Sci. Geogr. Sin. 22 (6), 705–711. https://doi.org/10.3969/j.issn.1000-0690.2002.06.012 (in Chinese with English abstract).
Zhang, K.L., Peng, W.Y., Yang, H.L., 2007. Soil erodibility and its estimation for agricultural soils in China. Acta Pedologica Sinica 44 (1), 7–13 (doi:CNKI:SUN:TRXB.0.2007-01-001, in Chinese with English abstract).
Zhang, S.W., Yang, Q., Ke, Ren, Z.P., Liu, H.Y., Li, J., Lu, G.Y., 2011. Dynamic analysis of land use in Ganzhou, Jiangxi province. Research of Soil and Water Conservation 18 (2), 53–56 (65, doi:CNKI:SUN:STBY.0.2011-02-013, in Chinese with English abstract).
Zhang, X.Y., Fan, J.R., Liu, Q., Xiong, D.H., 2017. The contribution of gully erosion to total sediment production in a small watershed in Southwest China. Phys. Geogr. 39 (3), 246–263. https://doi.org/10.1080/02723646.2017.1356114.
Zhang, S.Y., Zhuo, M.N., Xie, Z.Y., Yuan, Z.J., Wang, Y.T., Huang, B., Liao, Y.S., Li, D.Q., Wang, Y., 2020. Effects of near soil surface components on soil erosion on steep granite red soil colluvial deposits. Geoderma 365. https://doi.org/10.1016/j.geoderma.2020.114203.
Zhao, G.J., Klik, A., Mu, X.M., Wang, F., Gao, P., Sun, W.Y., 2015. Sediment yield estimation in a small watershed on the northern Loess Plateau, China. Geomorphology 241, 343–352. https://doi.org/10.1016/j.geomorph.2015.04.020.
Zhu, L., Han, X.J., Gao, Y., 2003. Climate warming and farming system reform. Agric. Econ. 5, 29. https://doi.org/10.3969/j.issn.1001-6139.2003.05.018 (in Chinese).